J|A|C|S ARTICLES

Published on Web 10/19/2010

Electrophoretic Mobilities of PEGylated Gold NPs

Tennyson L. Doane,[†] Yu Cheng,[†] Amir Babar,[†] Reghan J. Hill,*[,‡] and Clemens Burda*[,†]

Department of Chemistry, Case Western Reserve University, 10900 Euclid Avenue, Cleveland, Ohio, 44106, United States and Department of Chemical Engineering, McGill University, 3610 University Street, Montreal, Quebec, Canada, H3A 2B2

Received June 15, 2010; E-mail: reghan.hill@mcgill.ca; clemens.burda@case.edu

Abstract: Electromigration of nanoparticles (NPs) is relevant to many technological and biological applications. We correlate the experimentally observed electromigration of Au NPs with a closed-form theoretical model that furnishes key NP characteristics, including the previously *unknown* values of Au NP core ζ-potential, PEG-corona permeability, and particle-hydrogel friction coefficient. More generally, the theory furnishes new understanding of NP electromigration in complex environments, establishing a robust and predictive model to guide the design and characterization of functionalized NPs.

Introduction

Metal nanoparticles (NPs) are prevalent in many fields of nanotechnology, from electrodeposition,[1−4] and catalysis[5−8] to drug delivery[9] and bioimaging.[10,11] Gold NPs (Au NPs), in particular, are especially useful because of their adjustable size, shape, optical properties, and low toxicity.[12] In many applications, control of targeted NP transport is of prime importance. Research demonstrates that NP transport in diverse biological systems, such as cells,[9,13,14] embryos,[15,16] and plants,[17] brings with it the new challenge of designing materials with optimal transport properties. Due to low protein affinity[18] and cellular uptake,[19] poly(ethylene glycol) (PEG) coated NPs in particular have garnered considerable attention; at the same time, however, the bulky ligands alter NP mobility and physicochemical interaction with the local environment. Very few studies have been undertaken to determine the key forces acting on NPs during transport in complex media, especially under the influence of electric fields.[20]

A systematic approach to studying the mobility and physicochemical properties of NPs is gel electrophoresis. Several studies involving semiconductor quantum dots have shown how hydrodynamic radius,[21] ligand density,[22] and chain length influence mobility.[23] Other groups have used electrophoresis for the analysis of Au NPs, including glycocationic-modified Au NPs,[24,25] DNA−Au NP conjugates,[26−29] and human serum

[†] Case Western Reserve University.
[‡] McGill University.

(1) Quinn, B. M.; Dekker, C.; Lemay, S. G. *J. Am. Chem. Soc.* **2005**, *127*, 6146.
(2) Kim, S.-S.; Na, S.-I.; Jo, J.; Kim, D.-Y.; Nah, Y.-C. *Appl. Phys. Lett.* **2008**, *93*, 073307.
(3) Brown, P.; Kamat, P. V. *J. Am. Chem. Soc.* **2008**, *130*, 8890.
(4) Sakai, N.; Fujiwara, Y.; Arai, M.; Yu, K.; Tatsuma, T. *J. Electroanal. Chem.* **2009**, *628*, 7.
(5) de la Escosura-Muñiz, A.; Sánchez-Espineal, C.; Díaz-Fritas, B.; Gonazález-Fernández, A.; Maltez-da Costa, M.; Merkoçi, A. *Anal. Chem.* **2009**, *81*, 10268.
(6) Liu, Z.; Zhao, B.; Guo, C.; Sun, Y.; Xu, F.; Yang, H.; Li, Z. *J. Phys. Chem. C* **2009**, *113*, 16766.
(7) Zhao, D.; Wang, Y.-H.; Xu, B.-Q. *J. Phys. Chem. C* **2009**, *113*, 20903.
(8) Turner, M.; Golovko, V. B.; Vaughn, O. P. H.; Abdulkin, P.; Berenguer-Murcia, A.; Tikhov, M. S.; Johnson, B. F. G.; Lambert, R. M. *Nature* **2008**, *454*, 981.
(9) Cheng, Y.; Samia, A. C.; Li, J.; Kenney, M. E.; Resnick, A.; Burda, C. *Langmuir* **2010**, *26*, 4–2248.
(10) Pons, T.; Medintz, I. L.; Sapsford, K. E.; Higashiya, S.; Grimes, A. F.; English, D. S.; Mattoussi, H. *Nano Lett.* **2007**, *7* (10), 31574.
(11) Liu, X.; Knauer, M.; Ivleva, N. P.; Niessner, R.; Haisch, C. *Anal. Chem.* **2010**, *82*, 441.
(12) Sperling, R. A.; Gil, P. R.; Zhang, F.; Zanella, M.; Parak, W. *Chem. Soc. Rev.* **2008**, *37*, 1896.
(13) Rothen-Rutishauser, B.; Schürch, S.; Haenni, B.; Kapp, N.; Gehr, P. *Environ. Sci. Technol.* **2006**, *40*, 4353.
(14) Holbrook, R. D.; Murphy, K. E.; Morrow, J. B.; Cole, K. D. *Nat. Nanotechnol.* **2008**, *3*, 352.
(15) Lee, K. J.; Nallathamby, P. D.; Browning, L. M.; Osgood, C. J.; Xu, X.-H. N. *ACS Nano* **2007**, *1*, 133.
(16) Browning, L. M.; Lee, K. J.; Huang, T.; Nallathamby, P. D.; Lowman, J. E.; Xu, X.-H. N. *Nanoscale* **2009**, *1*, 138.
(17) Corredor, E.; Testillano, P. S.; Coronado, M.-J.; González-Melendi, P.; Fernández-Pacheco, R.; Marquina, C.; Ibarra, M. R.; de la Fuente, J. M.; Rubiales, D.; Pérez-de-Luque, A.; Risueño, M.-C. *BMC Plant Biol.* **2009**, *9*, 45.
(18) Verma, A.; Stellacci, F. *Small* **2010**, *6*, 12.
(19) Mok, H.; Bae, K. H.; Ahn, C.-H.; Park, T. G. *Langmuir* **2009**, *25*, 1645.
(20) Hanauer, M.; Pierrat, S.; Zins, I.; Lotz, A.; Sönnichsen, C. *Nano Lett.* **2007**, *7*, 2881.
(21) Pons, T.; Uyeda, H. T.; Medintz, I. L.; Mattoussi, H. *J. Phys. Chem. B* **2006**, *110*, 20308.
(22) Sperling, R. A.; Liedl, T.; Duhr, S.; Kudera, S.; Zanella, M.; Lin, C.-A. J.; Chang, W. H.; Braun, D.; Parak, W. J. *J. Phys. Chem. C* **2007**, *111*, 11552.
(23) Daou, T. J.; Li, L.; Reiss, P.; Josserand, V.; Texier, I. *Langmuir* **2009**, *25*, 3040.
(24) Ahmed, M.; Deng, Z.; Liu, S.; Lafrenie, R.; Kumar, A.; Narain, R. *Bioconjugate Chem.* **2009**, *20*, 2169.
(25) Ahmed, M.; Deng, Z.; Narain, R. *ACS Appl. Mater. Interfaces* **2009**, *1*, 1980.
(26) Claridge, S. A.; Liang, H. W.; Basu, S. R.; Fréchet, J. M. J.; Alivisatos, A. P. *Nano Lett.* **2008**, *8*, 1202.
(27) Zanchet, D.; Micheel, C. M.; Parak, W. J.; Gerion, D.; Williams, S. C.; Alivisatos, A. P. *J. Phys. Chem. B* **2002**, *106*, 11758.
(28) Zanchet, D.; Micheel, C. M.; Parak, W. J.; Gerion, D.; Alivisatos, A. P. *Nano Lett.* **2001**, *1*, 32.
(29) Parak, W. J.; Pellegrino, T.; Micheel, C. M.; Gerion, D.; Williams, S. C.; Alivisatos, A. P. *Nano Lett.* **2003**, *3*, 33.

10.1021/ja1049093

albumin-modified Au NPs.[30] Hanauer et al. used electrophoresis for efficient separation of PEGylated Ag and Au NPs based on size, shape, and functionalization.[20] Gel electrophoresis has also been used to determine the extent to which a Au NP surface is capped by monofunctional methoxy-PEG (mPEG-SH) ligands (ligand density).[31,32]

In this paper, we describe gel electrophoresis experiments and a theoretical model that quantify the role of the PEG−ligand molecular weight (MW) on NP transport in agarose gels. Increasing the PEG−ligand MW and hydrodynamic radius directly influences the electrophoretic mobility. Our study explains observations in the literature where PEGylated Au NPs with negative ζ-potentials migrated toward negative electrodes. The effects of ionic strength, gel density, agarose type, and electric field strength are systematically studied to enhance the control of targeted NP transport. Our results quantify how NP PEGylation affects the balance of electrophoretic, electroosmotic, and frictional coupling forces.

Experimental Section

Thirty percent $HAuCl_4$, $NaBH_4$, dodecylamine (DDA), and Vitamin B_{12} were purchased from Sigma Aldrich and used without further purification. Monofunctional methoxy polyethylene glycol thiol (HS-mPEG) of different lengths was purchased from Laysam Bio Inc. 10× TAE Buffer (Fischer) was diluted to 1× using deionized water, and the gels were loaded using glycerol (Baker).

Au NPs were formed using a variation of the Brust-Schiffrin method,[33] which has been described earlier.[34] Ligand exchange of different molecular weight mPEG-SH ligands was conducted in $CHCl_3$. The HS-mPEG−Au NPs were then further purified by suspension in water and centrifugation through a 10 kDa molecular weight cut off membrane separated centrifuge tube (Viva Sciences). This process was repeated 10 times to ensure purity. Samples were then diluted in water, and the UV−vis spectrum was measured (Cary 50 Bio). The solutions were adjusted to have the same Au NP concentration (2.1 μM). Stock vitamin B_{12} was prepared with a concentration of ∼3.8 mM to have a similar optical absorbance as the Au NP samples (extinction coefficients of 1.5×10^7 and 8.5×10^3 M^{-1} cm^{-1} for Au NPs[34] and vitamin B_{12},[35] respectively).

Agarose gels of varying concentration were prepared by dissolving agarose powder (Invitrogen, Ultra Pure) in buffer solution, heated to boiling using a microwave, and then poured into 13.8 × 11.8 cm plates (Owl Separation Systems). The gels were allowed to set for 45−60 min. Gels were then realigned in the electrophoresis wells and submerged in buffer solution. The ionic strength of the Tris Acetate EDTA (TAE) running buffer was calculated using methods similar to Hseih et al.[36] using equilibrium calculations for the relevant ions[37] (1× TAE: 43 mM Tris [pK_a 8.06], 43 mM acetate [pK_a 4.76], 1 mM EDTA [pK_{a1} 2.00, pK_{a2} 2.69, pK_{a3} 6.13, pK_{a4} 10.37], and 2 mM Na^+). It is conventional to write the buffer ionic strength in terms of a dilution factor in gel electrophoresis experiments. The concentrated 10× TAE buffer is diluted to the desired concentration, where 1× TAE is ∼42 mM ionic strength. Variable times and voltages were adjusted with a Bio-RAW Power Pac Basic/3000 power supply. Samples were prepared for injection by mixing 5 μL of water, 10 μL of NP solution, and 5 μL of glycerol together, for final Au NP and Vitamin B_{12} concentrations of ∼1 μM and ∼1.9 mM, respectively. Gel images were obtained using a commercial digital camera (Olympus Camedia D-595) on an optics bench with a fixed frame for consistent photography. Distances were measured with a small ruler, achieving 0.5 mm resolution.

Table 1. Hydrodynamic Diameters (DLS) and ζ-Potentials (DLS-microelectrophoresis) for PEGylated Au NPs[a] with Varying PEG−Ligand MW

PEG MW (kDa)	Hydrodynamic diameter, d_{hydro}[b] (nm)	ζ-potential[c] (mV)
1	17.6 ± 2.0	−7.7 ± 3.3
2	25.7 ± 2.0	−2.4 ± 3.8
5	37.6 ± 1.1	−5.4 ± 2.1
10	52.5 ± 3.8	−0.1 ± 0.0

[a] Au NP diameters are 5.7 ± 2.0 nm from TEM analysis. [b] On the basis of three measurements from three different instruments. [c] Averages from DLS-microelectrophoresis using Smoluchowski's formula, with 10 V/cm and pH 5.5.

Dynamic light scattering (DLS) measurements were obtained on a BI-200SM laser light scattering goniometer with a BI 9000AT autocorrelator (Brookhaven Instruments Corp.). A He−Ne laser (632.8 nm, 15 mW) was used for the scattering, and the detection angle was 90°. The sampling duration was 30−60 min with a 200 μm pinhole. The CONTIN method was used to analyze the data. All measurements were performed at 25 °C. Further analysis was undertaken on 1 kDa and 2 kDa PEG-capped Au NPs by Brookhaven Instruments and on all samples with a NICOMP 380 DLS/Zeta instrument (Particle Sizing Systems). ζ-Potential measurements were undertaken using a NICOMP 380 DLS/Zeta instrument (Particle Sizing Systems), with different field strengths (3 and 10 V/cm) and different ionic strengths tested (0.1 mM and 10 mM). Transmission electron microscopy (TEM) was performed using a JEOL JEM 1200 EX electron microscope and analyzed as previously reported.[34]

Results

Au NPs with an average diameter of 5.7 nm were capped with 1, 2, 5, and 10 kDa MW mPEG-SH as capping ligand. Dynamic light scattering (DLS) measurements reveal an increasing NP hydrodynamic radius with increasing mPEG-SH MW, as shown in Table 1. NP ζ-potentials from DLS-microelectrophoresis decrease from a low value of approximately −8 mV with 1 kDa PEG to vanishingly small values with increasing PEG MW, although the trend is not monotonic. Thermal gravimetric analysis (TGA) of 2 kDa mPEG-SH-capped Au NPs indicate about 84% surface coverage (0.42 nm^2/PEG compared to 0.35 nm^2/PEG for thiolated PEG on a 2.8 nm diameter Au colloid reported by Wuelfing et al.[38]).

A standard electrophoresis experiment using a 1% agarose gel with 1× TAE buffer run at 80 V for 4 h is shown in Figure 1a. Increasing the PEG MW (from 1 to 10 kDa) produces significant changes in mobility, with the 1 kDa Au NPs moving toward the positive electrode and the 5 and 10 kDa PEGylated Au NPs moving toward the negative electrode. These results agree with other literature reports.[20,31,32] In addition, vitamin B_{12}, an uncharged electroosmotic flow tracer, also migrates toward the negative potential, indicating a negatively charged agarose skeleton.[20] Figure 1a demonstrates that increasing the PEG ligand MW eventually leads to migration in the same

(30) Lôpez-Viota, J.; Mandal, S.; Delgado, A.; Toca-Herrera, J. L.; Möller, M.; Zanuttin, F.; Balestrino, M.; Krol, S. *J. Colloid Interface Sci.* **2009**, *332*, 215.
(31) Liu, Y.; Shipton, M. K.; Ryan, J.; Kaufman, E. D.; Franzen, S.; Feldheim, D. L. *Anal. Chem.* **2007**, *79*, 2221.
(32) Perrault, S. D.; Chan, W. C. W. *J. Am. Chem. Soc.* **2009**, *131*, 17042.
(33) Brust, M.; Walker, M.; Bethell, D.; Schiffrin, D. J.; Whyman, R. *J. Chem. Soc., Chem. Commun.* **1994**, *7*, 801.
(34) Cheng, Y.; Samia, A. C.; Meyers, J. D.; Panagopoulos, I.; Fei, B.; Burda, C. *J. Am. Chem. Soc.* **2008**, *130*, 10643.
(35) Watanabe, F.; Abe, K.; Fujita, T.; Goto, M.; Hiemori, M.; Nakano, Y. *J. Agric. Food Chem.* **1998**, *46*, 206.
(36) Hsieh, C.-C.; Balducci, A.; Doyle, P. S. *Nano Lett.* **2008**, *8*, 1683.
(37) Harris, D. *Quantitative Chemical Analysis*, 7th ed.; W. H. Freeman and Co.: New York, 2007; p 174.
(38) Wuelfing, W. P.; Gross, S. M.; Miles, D. T.; Murray, R. W. *J. Am. Chem. Soc.* **1998**, *120*, 12696.

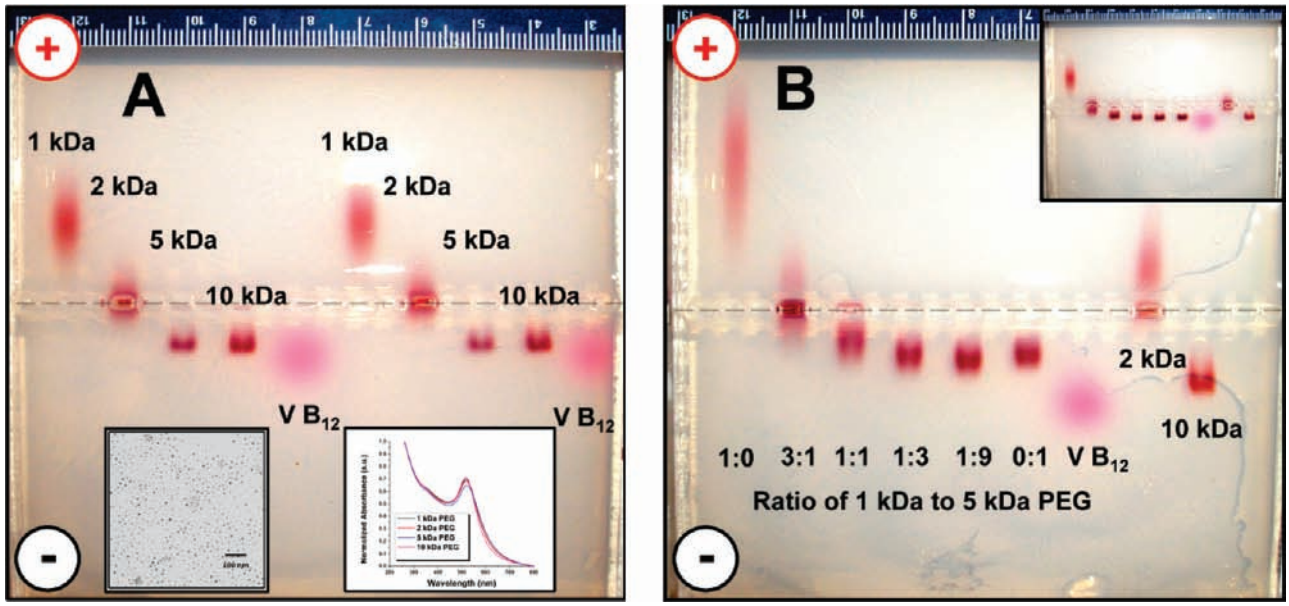

Figure 1. (A) Gel electrophoresis (1% agarose) of 1 k, 2 k, 5 k, and 10 kDa PEGylated Au NPs in 1× (42 mM) TAE buffer at 80 V for 4 h. Each time two identical samples were run for comparison. (Insets) Representative TEM of Au NPs used, and the UV−vis spectra of the PEGylated Au NPs. (B) Electrophoresis of Au NPs capped with varying ratios from 1 kDa PEG to 5 kDa PEG in a 1% w/v agarose at 80 V for 4 h with 0.25× (10.5 mM) TAE buffer. Vitamin B_{12}, 2 kDa PEG, and 10 kDa PEGylated Au NPs are shown for comparison. (Inset) Same experiment but with 1× (42 mM) TAE buffer.

direction as vitamin B_{12}. This might be erroneously interpreted as a change in sign of the NP charge. However, we will show that the change in apparent ζ-potential is due to an increase in the hydrodynamic size and the accompanying increase in the hydrodynamic screening of the Au NP core by the PEG corona. Simultaneously, longer PEG chains increase hydrodynamic and frictional drag forces on the PEGylated Au NPs, thereby diminishing the electrical force and making the NPs highly susceptible to electroosmotic flow and steric interaction with the gel.

Interestingly, the NP electrophoretic mobility μ_T can be "tuned" by varying the PEG MW, as evident from the "stationary" 2 kDa PEGylated Au NPs in our standardized experiments. TEM and UV−vis absorption spectra (insets in Figure 1a) reveal well-dispersed NPs, excluding aggregation as a factor that modulates NP mobilities.

To further assess how the NP mobility depends on PEG MW, we used four different ratios from 1 to 5 kDa PEG via standard ligand exchange. Increasing the ratio of 5 kDa PEG reverses the mobility from the negative electrode toward the positive electrode, as illustrated in Figure 1b. The inset of Figure 1b shows the same experiment with 1× TAE buffer. Noteworthy is that a more dilute 0.25× TAE buffer enhances band separation, thereby distinguishing 1−5 kDa ratios of PEGylated Au NPs. We attribute the enhanced band resolution to changes in the diffuse double-layer thickness, as quantified by the Debye length, κ^{-1}. Decreasing the ionic strength increases the Debye length, leading to lower PEG−ligand MW NPs migrating toward the positive electrode. Thus, NPs with the same charge migrate according to their PEG layer thickness and permeability. Conversely, increasing the ionic strength decreases the Debye length and apparent charge, so the NP mobility primarily reflects the hydrogel electroosmotic flow mobility μ_{EOF}, with secondary influences from frictional and hydrodynamic coupling with the hydrogel skeleton.

The results in Figure 2 summarize how the experimental parameters affect Au NP electrophoretic mobilities. Increasing the voltage from 60 to 120 V (Figure 2A) produces a relatively small (from ∼0.06 to 0.14 $\mu m\ V^{-1}\ cm\ s^{-1}$) increase in particle mobilities. Classical (linear) theory predicts mobilities that are independent of voltage at the low electric field strengths prevailing. The increase is more pronounced for the vitamin B_{12} tracer and NPs with higher PEG MW, suggesting a disproportionate enhancement of the hydrogel electroosmotic flow with electric field strength. This might be due to changes in pH and, thus, gel ionization brought about by Joule heating or pH changes from electrochemical reactions at the electrodes. It is also possible that the hydrogel microstructure is modulated by the electroosmotic flow. For example, long agarose filaments with free ends might adopt increasingly more streamlined configurations in the stronger electroosmotic flow that accompanies an increase in voltage. Increasing the agarose concentration from 0.5 to 2.0 w/v % (Figure 2B) generally decreases the mobility of all PEGylated Au NPs and the vitamin B_{12} tracer. The same experiment with a lower ionic strength (10.5 mM) buffer reveals that the 5 kDa PEGylated Au NPs migrate shorter distances in the positive direction than 10 kDa PEGylated Au NPs at higher agarose concentrations with the same electric field strength. This highlights the role of steric interaction (also termed frictional coupling) between the NPs and the hydrogel skeleton. Increasing the ionic strength from 10.5 to 42 mM (Figure 2C) decreases the electrophoretic mobility of all NPs. This reflects the role of the diffuse double-layer thickness on the electroosmotic flow driven by the particle and hydrogel counter charge. Finally, we conducted experiments with various types of agarose to discern how gel structure influences NP migration (Figure 2D). Variations in the electroosmotic flow, as indicated by the vitamin B_{12} tracer mobilities in Figure 2D, are in good agreement with the values reported

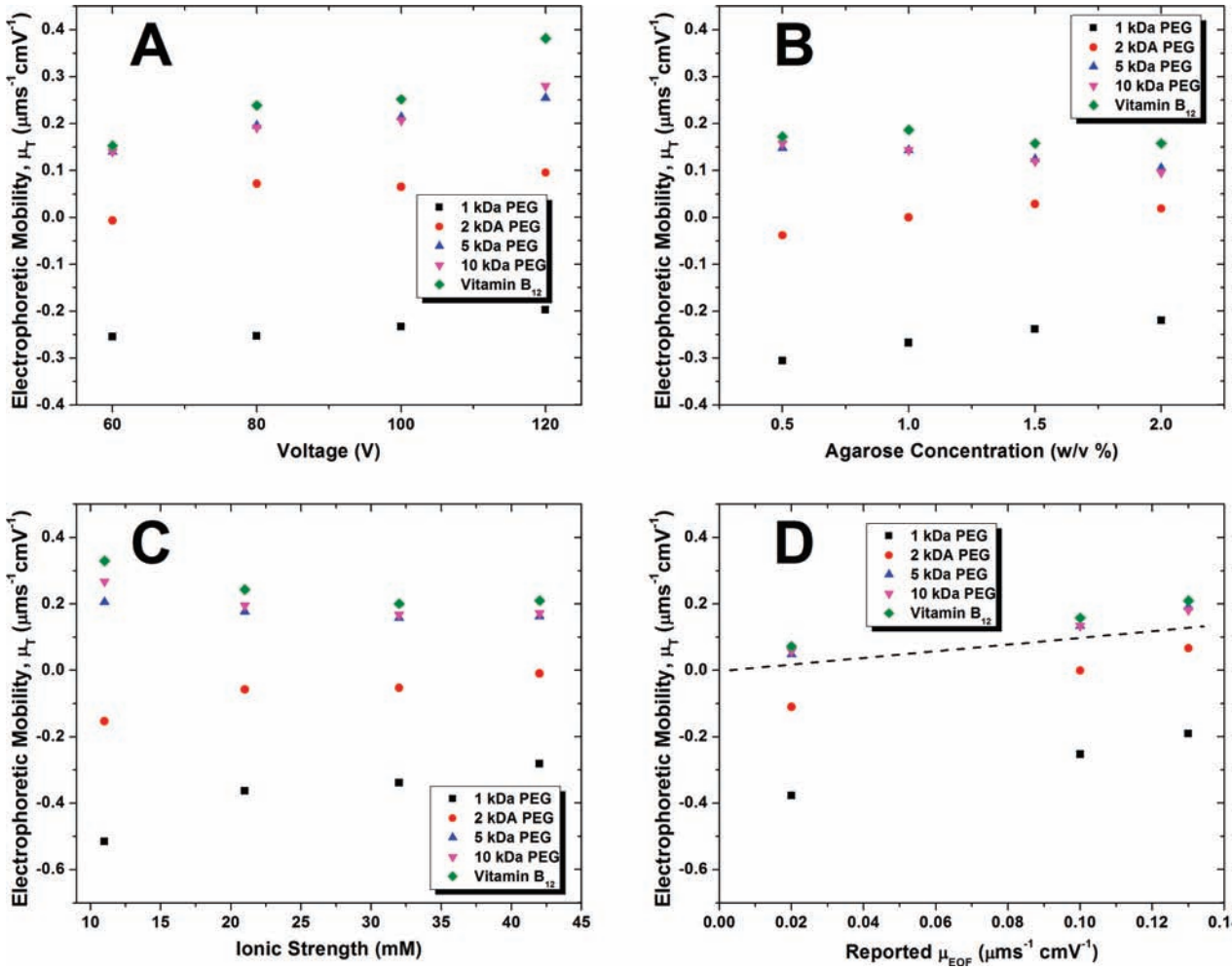

Figure 2. Dependence of NP electrophoretic mobility μ_T on (A) voltage, (B) agarose concentration, (C) ionic strength, and (D) agarose type. The hydrogel electroosmotic mobility, μ_{EOF}, in D is provided by the manufacturer; the line is the mobility of an ideal passive tracer with $\mu_T = \mu_{EOF}$, which is well represented by the vitamin B_{12} mobilities. Standard run was 1% Invitrogen Ultra Pure Agarose, 1× TAE (42 mM ionic strength), pH 8.3, at 80 V for 4 h. Average error is 0.01 μm s^{-1} cm V^{-1} for mobility measurements.

by the manufacturer (straight line indicates $\mu_T = \mu_{EOF}$) with NP mobilities varying proportionally.

Experiments with lower voltages, necessitating longer run times (40−60 V, >16 h), also yield mobilities that increase linearly with voltage. With increasing agarose concentration, all Au NP mobilities slightly decreased (Figure 2b). The agarose concentration directly alters the size of pores through which NPs migrate. Several groups have attempted to ascertain the physical nature of the gel microstructure using techniques such as atomic force microscopy (AFM).[39] Recently, Stellwagen and Stellwagen noted that the typical "pore" radius for a 1% agarose gel is ∼100 nm.[40] Thus, we expect the accompanying frictional coupling to play an increasingly important role at higher agarose concentrations. Note that even the vitamin B_{12}, which has a hydrodynamic radius of only 0.84 nm,[41] slows down slightly with increasing agarose concentration. For these particles, however, the decrease in mobility can be attributed to the lower gel permeability (increased skeleton drag), which, in turn, is due to enhanced hydrodynamic interaction between increasingly concentrated agarose filaments. This argument is considerably strengthened by the ostensible (longitudinal and transverse) broadening of the vitamin B_{12} patches, which is practically independent of hydrogel concentration.

Discussion

The foregoing phenomenological arguments are supported by the following quantitative model for the electrophoretic mobility of spherical NPs dispersed in charged (polyelectrolyte) hydrogel skeletons. First, we consider a crude but illustrative model of a NP in an ideal charged capillary with a longitudinal electric field E. Electrophoretic translation of the particle with respect to the stationary capillary can generally be considered as the superposition of the intrinsic NP electrophoretic velocity U_p in an unbounded, stagnant electrolyte and the (average) electroosmotic fluid velocity U_c of the electrolyte in the charged capillary. For an ideal colloidal sphere with low ζ-potential $|\zeta_p| < k_BT/e$, the intrinsic electrophoretic mobility falls between the well-known Smoluchowski and Hückel limits, depending on the parameter κa, which is the ratio of the particle radius a to the

(39) Pernodet, N.; Maaloum, M.; Tinland, B. *Electrophoresis* **1997**, *18*, 55.
(40) Stellwagen, N. C.; Stellwagen, E. *J. Chromatogr. A* **2009**, *1216*, 1917.
(41) Harland, R. S.; Peppas, N. A. *Colloid Polym. Sci.* **1989**, *267*, 218.

Debye length κ^{-1}. Henry's formula for the intrinsic particle mobility,[42] valid for any value of ka, is

$$U_p/E = (\varepsilon\varepsilon_0\zeta_p/\eta)f_H(\kappa a) \quad (|\zeta_p| < k_BT/e) \tag{1}$$

where $\varepsilon\varepsilon_0$ is the electrolyte dielectric constant, η is the electrolyte shear viscosity, and $2/3 < f_H < 1$ is a dimensionless function of κa involving exponential integrals. Similarly, for an ideal circular capillary with low surface ζ-potential $|\zeta_c| < k_BT/e$, the average electroosmotic mobility falls between limits set by the parameter κR, which is the ratio of the cylinder radius R to the Debye length. Paralleling Henry's formula, Rice and Whitehead derived a formula for the electroosmotic mobility[43] valid for any κR (here in the absence of a pressure gradient)

$$U_c/E = -(\varepsilon\varepsilon_0\zeta_c/\eta)f_{RW}(\kappa R) \quad (|\zeta_c| < k_BT/e) \tag{2}$$

where $0 < f_{RW} < 1$ is a dimensionless function of κR involving modified Bessel functions. Accordingly, the absolute or apparent particle electrophoretic mobility in a capillary tube is simply

$$U/E = U_p/E + U_c/E = \varepsilon\varepsilon_0[\zeta_p f_H(\kappa a) - \zeta_c f_{RW}(\kappa R)]/\eta \tag{3}$$

While this simple model neglects steric, electrical, and hydrodynamic interactions between the particle and capillary wall, it clearly illustrates how the sign and magnitude of $\mu_T = U/E$ depends on the particle and capillary-wall ζ-potentials. One must also bear in mind that the ζ-potentials, while linear in their respective surface charge densities, depend on κ when the surface charge is fixed. Under these conditions, Gauss's law shows that ζ-potentials vanish with increasing ionic strength (or κ).

The foregoing model also neglects the effect that an uncharged polymer grafted (or adsorbed) onto the charged surface of a NP has on the intrinsic electrophoretic mobility. Indeed, there have been numerous studies addressing the electrophoretic mobility of *soft* colloidal particles. Among many analytical solutions for soft colloidal spheres, Ohshima derived a formula for the mobility that can be written[44]

$$U/U_0 = f_O(\kappa L, l/L) < 1 \tag{4}$$

for a weakly charged ($|\zeta_p| < k_BT/e$), impenetrable sphere bearing a thin uncharged polymer coating with $\kappa a \gg 1$ and layer thickness $L \ll a$. Here, U_0 is the particle electrophoretic velocity without the polymer coating and l (square root of the Darcy permeability) is the so-called Brinkman screening length.[45] Ohshima's formula quantifies how increasing the polymer-layer thickness and decreasing its permeability decrease the electrophoretic mobility (crudely considered as decreasing the effective ζ-potential) without actually changing the particle charge. Unfortunately, an explicit formula valid for $\kappa a < 1$ with arbitrary κL and l/L does not exist, but numerical solutions of the electrokinetic model have been reported.[46,47] In general, these exhibit the qualitative trends captured by eq 4.[44]

To quantitatively interpret and correlate our experimental data, we extended the foregoing electrokinetic model to a spherical NP embedded in a polyelectrolyte hydrogel, itself modeled as a charged porous medium. In this manner, we account for the hydrodynamic interaction of the particle with the hydrogel, including the hydrodynamic drag required for the particle to drive fluid through the surrounding polymer skeleton. Our model also accounts for the disturbance of the particle to the electroosmotic flow driven by the electric field through the hydrogel, the electric-field-induced flow within the diffuse double layer that envelops the NP, and frictional coupling of the particle and hydrogel. It also captures how changes in hydrogel density and charge influence particle migration, as well as the influences of electrolyte concentration, and particle size and charge. Fitting this model to experimental data not only captures the qualitative trends with remarkable fidelity but also furnishes acceptable values for several otherwise unknown model parameters. Accordingly, we believe the model holds considerable promise for understanding and predicting the transport of PEGylated NPs in complex media.

We consider a charged colloidal sphere undergoing steady electromigration through a charged hydrogel, which we model as a Brinkman medium.[45] We write the forces on the sphere by superposing the forces in two simpler situations. In the so-called U problem, the sphere is translated through the gel with velocity $\boldsymbol{U}$ in the absence of the applied electric field. The particle experiences a hydrodynamic drag force and, in general, a frictional coupling force due to steric interaction with the hydrogel skeleton. Accordingly, we write

$$\boldsymbol{F}^U = -2\pi\eta a f_B(a/l_g)\boldsymbol{U} - 2\pi a^2 n_g k_B T u_f^{-1}\boldsymbol{U} \tag{5}$$

where

$$f_B(a/l_g) = (a/l_g)^2[1 + 3(l_g/a) + 3(l_g/a)^2] \tag{6}$$

Here, η is the solvent shear viscosity, a is the sphere radius, l_g is the gel hydrodynamic permeability, n_g is the hydrogel segment number density, k_BT is the thermal energy, and u_f is a characteristic frictional-coupling velocity that integrates two molecular length scales and one molecular relaxation time scale. Note that f_B (a/l_g) is a dimensionless function attributed to Brinkman;[45,48] it recovers the well-known Stokes hydrodynamic drag force ($f_B \to 3$) as $l_g a \to \infty$ and the so-called Darcy drag force [$f_B \to (a/l_g)^2$] as $l_g/a \to 0$.

In the so-called E problem, the sphere is held fixed in the gel while subjected to an applied electric field $\boldsymbol{E}$. The particle experiences hydrodynamic and electrical forces due to the intrinsic particle charge and the electroosmotic flows driven by the particle and hydrogel counter charge. To solve this problem, we adopt the well-known Debye−Hückel approximation, which permits superposition of the force $\boldsymbol{F}^{E(1)}$ on a charged sphere embedded in an uncharged hydrogel and the force $\boldsymbol{F}^{E(2)}$ on an uncharged sphere embedded in a charged hydrogel with a fixed (apparent) charge density ρ_f. Accordingly, we write

$$\boldsymbol{F}^E = \boldsymbol{F}^{E(1)} + \boldsymbol{F}^{E(2)} \tag{7}$$

where

$$\boldsymbol{F}^{E(1)} = 4\pi\varepsilon\varepsilon_0\zeta a\boldsymbol{E} \quad (\kappa a \le 1, |\zeta| \le 2k_BT/e) \tag{8}$$

and

(42) Henry, D. C. *Proc. R. Soc. London A* **1931**, *133*, 106.
(43) Rice, C. L.; Whitehead, R. *J. Phys. Chem.* **1965**, *69*, 4017.
(44) Ohshima, H. *J. Colloid Interface Sci.* **1989**, *130*, 281.
(45) Brinkman, H. C. *Appl. Sci. Res. A* **1947**, *1*, 27.
(46) Hill, R. J.; Saville, D. A.; Russel, W. B. *J. Colloid Interface Sci.* **2003**, *258*, 56.
(47) Hill, R. J.; Saville, D. A. *Colloids Surf. A.* **2005**, *267*, 31.
(48) Hill, R. J. *J. Fluid Mech.* **2006**, *551*, 405.

$$\boldsymbol{F}^{E(2)} = -2\pi\eta a f_B(a/l_g) l_g^2 \eta^{-1} \rho_f \boldsymbol{E} \tag{9}$$

Here, $\varepsilon\varepsilon_0$ is the solvent dielectric constant and ζ is the particle ζ-potential. Note that eq 8, which is strictly valid when the particle radius is smaller than the Debye length κ^{-1}, is the bare Coulomb force. In general, however, $\boldsymbol{F}^{E(1)}$ also depends on l_g/a and is available from numerical solutions of the full electrokinetic model.[48,49]

Superposing the forces in the foregoing U and E problems to satisfy the particle equation of motion

$$\boldsymbol{F}^U + \boldsymbol{F}^E = 0 \tag{10}$$

furnishes the electrophoretic mobility (μ_T). Scaling this with the hydrogel electroosmotic mobility, $\mu_{EOF} = \rho_f l_g^2/\eta$, gives

$$\frac{\mu_T \eta}{l_g^2 \rho_f} = \frac{\Pi_1/f_B(a/l_g) - 1}{1 + \Pi_2/[F(\phi_g) f_B(a/l_g)]} \tag{11}$$

where the dimensionless parameters

$$\Pi_1 = \frac{2\varepsilon\varepsilon_0 \zeta}{l_g^2 p_f} \text{ and } \Pi_2 = \frac{k_B T a}{l_g^2 6\pi\eta a_g u_f} \tag{12}$$

are, respectively, the ratio of the Hückel particle mobility to the hydrogel electroosmotic mobility and the ratio of the frictional coupling force to the Stokes drag force. The dimensionless hydrogel-segment drag coefficient $F(\phi_g) \approx 1$, which depends on the hydrodynamic volume fraction (ϕ_g), is addressed below. Equation 11 is the principal theoretical relationship adopted in this work to interpret the experimental data. However, to adapt eq 11 for soft NPs, we replace the particle radius a above by the soft NP hydrodynamic radius $a_h = a_c + L_h$. Here, a_c is the gold-core radius and L_h is the PEG-coating hydrodynamic layer thickness. In addition to modeling the layer as an uncharged, uniform Brinkman medium, we make the reasonable assumption that $L_h \approx L - l_p$, where L is the polymer layer thickness and l_p is its hydrodynamic permeability.[47] Additionally, we replace the particle ζ-potential above by the electrostatic potential at the soft NP hydrodynamic shear plane. Recall, Ohshima[44] derived a formula for the electrophoretic mobility of soft composite spheres with $\kappa(a_c + L) \gg 1$ and $L \ll a_c$. Moreover, with the Debye−Hückel approximation, the mobility is proportional to the electrostatic potential ζ_c (gold-core ζ-potential) at the particle−polymer interface. Note that ζ_c is the ζ-potential of a hypothetical particle without a polymer coating. On gold surfaces, the negative potential is due to anion adsorption, which,[50] from a large body of literature that spans 25 years,[51] has been shown to be controlled by both chemical and electronic factors.[50] Using ζ_c, we adopt Ohshima's mobility formula to write the effective NP ζ-potential as

$$\zeta = \frac{\zeta_c}{1 - (\kappa l_p)^{-2}} \left[\frac{1}{\cos(L/l_p)} - \frac{e^{-\kappa L}}{\kappa l_p} \left(\frac{1}{\kappa l_p} + \tanh(L/l_p) \right) \right] \tag{13}$$

From numerically exact solutions of the full electrokinetic model for soft spheres,[47] this formula captures—at least qualitatively—how the effective charge of the soft composite sphere is modulated by the polymer-layer thickness L, hydrodynamic permeability l_p^2, and Debye length κ^{-1}.

To express the hydrodynamic permeabilities of the hydrogels and NP corona in terms of their respective segment densities (n_g and n_p) and segment hydrodynamic radii (a_g and a_p) for the gel and particle, respectively, we model each porous medium as a dilute, random configuration of spherical Stokes resistance centers. Accordingly

$$l_g^2 = \frac{1}{6\pi n_g a_g F(\phi_g)} \text{ and } l_p^2 = \frac{1}{6\pi n_p a_p F(\phi_p)} \tag{14}$$

where the segment drag coefficient[45]

$$F = 1 + 3(\phi/2)^{1/2} \tag{15}$$

when the hydrodynamic volume fraction $\phi = \phi_g = n_g(4/3)\pi a_g^3 \ll 1$ or $\phi = \phi_p = n_p(4/3)\pi a_p^3 \ll 1$. Note that terminally anchored PEG chains can be modeled with a (statistical) segment hydrodynamic radius $a_p \approx 0.0175$ nm and accompanying segment MW $m_p \approx 71$ Da.[52] Thus, the foregoing relationships permit l_p to be calculated from knowledge of the hydrodynamic polymer layer thickness L_h (available from DLS and TEM), PEG−ligand MW M_{PEG}, and the number of grafted PEG chains N_{PEG}. From DLS and TEM, we obtain an empirical formula where $L_h \approx 6.0\ M_{PEG}^{0.61}$ nm (with M_{PEG} in kDa). Note that our empirical power-law exponent 0.61 is very close to the theoretical value 3/5 that prevails for uncharged polymer brushes in the limit of high grafting-surface curvature.[53] Thus, our data indicate densely grafted chains on an highly curved surface ($L_h/a_c > 1$). Moreover, from thermogravimetric analysis (TGA) of 2 kDa PEGylated Au NPs, we obtain a ligand grafting density $\Gamma_{PEG} \approx 2.4$ nm^{-2}.

When fitting the model to experimental electrophoresis data, we adopted a constant Au NP core radius $a_c \approx 2.87$ nm, corresponding to the average value from TEM images of particles with four different PEG MWs. With the foregoing grafting density, it follows that $N_{PEG} \approx 246$. Table 2 summarizes the measured and calculated geometrical and hydrodynamic characteristics of the various PEGylated Au NPs. Note that the calculated layer thicknesses L are larger than the experimental and fitted hydrodynamic thickness L_h by the respective Brinkman screening length, l_p. Moreover, l_p increases with the PEG MW, since the layer thickness increases in a manner where the polymer segment density n_p decreases with increasing MW. The ratio L/l_p furnishes a dimensionless measure of the hydrody-

Table 2. Calculated Hydrodynamic Draining Characteristics of PEGylated NPs[a]

M_{PEG} (kDa)	L_h (DIS/TEM) (nm)	L_h (nm)	L (nm)	l_p (nm)	L/l_p
1	5.5	6	8.2	2.2	3.7
2	10.4	9.2	11.5	2.3	5.0
5	16	16	18.7	2.7	6.9
10	23.4	24.4	27.7	3.2	8.6

[a] Calculations are undertaken with fixed Au NP (core) radius $a_c = 2.87$ nm, fixed PEG grafting density $\Gamma_{PEG} \approx 2.4$ nm^{-2}, and other parameters detailed in the text. L_h = PEG hydrodynamic layer thickness, where $L_h \approx 6.0\ M_{PEG}^{0.61}$ nm (with M_{PEG} in kDa). L = PEG layer thickness, where $L_h \approx L - l_p$. l_p = PEG layer Brinkman screening length (refer to eq 14).

(49) Hill, R. J. *Phys. Fluids* **2006**, *18*, 043103.
(50) Tripkovic, D. V.; Strmcnik, D.; van der Vliet, D.; Stamenkovic, V.; Markovic, N. M. *Faraday Discuss.* **2008**, *140*, 25.
(51) Conway, B. E. In *Progress in Surface Science*; Davison, S., Ed.; Pergamon Press: Fairview Park, NY, 1984; p 1.
(52) Hill, R. J. *Phys. Rev. E* **2004**, *70*, 051406.
(53) Biver, C.; Hariharan, R.; Mays, J.; Russel, W. B. *Macromolecules* **1997**, *30*, 1787.

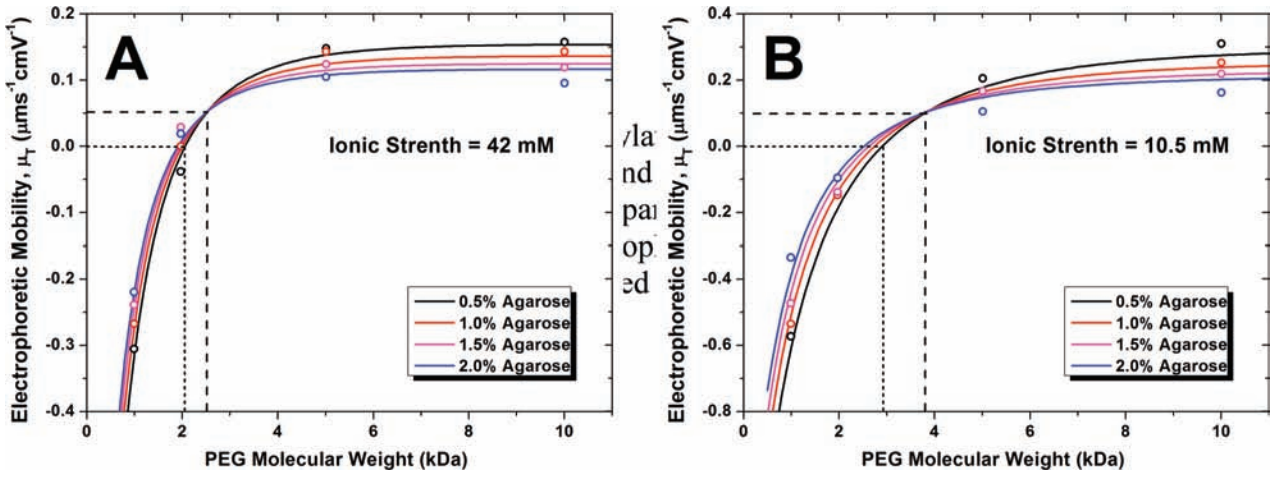

Figure 3. Electrophoretic mobility of PEGylated Au NPs versus PEG−ligand MW for several agarose gel concentrations with (A) 42 and (B) 10.5 mM ionic strength TAE buffer with $M_g = 103$ kDa. Measurements (symbols) are compared to theory (lines) with parameters provided in Table 3. Note the PEG MWs yielding zero electrophoretic mobility (dotted lines) and mobilities that are independent of agarose concentration (dashed lines). Average error is 0.01 μm s^{-1} cm V^{-1} for mobility measurements.

namic permeability. Interestingly, even though the layer density decreases with increasing MW, l_p increases more slowly than L, so $L/L_h \rightarrow 1$ as $M_{PEG} \rightarrow \infty$.

Combining the foregoing models furnishes a complete electrokinetic model with the following *unknown*, independent parameters: M_g, a_g, and hydrogel segment valence z_g characterize the hydrogels, κ^{-1} characterizes the electrolyte, ζ_c characterizes the NPs, and u_f characterizes the particle-hydrogel frictional coupling. We obtained these parameters from the experiments using the following two-step fitting methodology. First, we chose a value of M_g and obtained a_g and z_g by nonlinear least-squares fitting of the model to the measured electrophoretic mobilities of vitamin B_{12} in agarose gels with three concentrations and a fixed electrolyte. To help identify the correct order of magnitude for M_g, we note that Johnson and Deen[54] carefully measured the hydrodynamic permeability of 2% agarose gels, reporting $l_g \approx 24.8$ nm. Thus, to achieve comparable permeabilities from fitting the model to electrophoresis data, we find $M_g \approx 10^3$ kDa. Next, the NP (vitamin B_{12}) is taken to be an uncharged ($\zeta_{B12} = 0$) sphere with a hydrodynamic radius $a_{B12} \approx 0.84$ nm that is independently obtained from the literature.[41] We then fitted the model to the measured electrophoretic mobilities of PEGylated Au NPs with four different PEG MWs in the same three agarose gels and electrolyte. This specified the remaining parameters: κ^{-1}, ζ_c, and u_f.

The model predictions of NP electrophoretic mobilities are compared with experimental data in Figure 3, where the agarose segment MW $M_g = 10^3$ kDa. The accompanying parameters are summarized in Table 3 for fits undertaken with both $M_g = 10^3$ and 10^4 kDa. Our results show that an order of magnitude change in the choice of M_g has a very small change in the product $u_f \times M_g$. This indicates that the particle-hydrogel frictional coupling force (eq 5) depends on the total gel concentration, $c \approx n_g M_g$, rather than n_g. Thus, the PEG chains interact with all hydrogel monomer segments, not just the much larger, course-grained segments with molecular weight M_g.

We fitted the model to two sets of experimental data. The 1× TAE buffer data has an electrolyte nominal ionic strength of $I \approx 40$ mM, whereas the 0.25× TAE buffer data has $I \approx 10$ mM. Thus, noteworthy of the fitted Debye lengths is that they vary by a factor of about two, in excellent correspondence with the factor of about four in the accompanying ionic strengths. We note that the best-fit values of ζ_c from −59 to −64 mV are, as expected, considerably higher than the vanishingly small ζ-potentials of the NPs ascertained from DLS-microelectrophoresis (see Table 1). Recall, this is due to the hydrodynamic screening of the PEG coatings, as indicated by eq 13. Note that the fitted values of ζ_c are practically independent of M_g, which is to be expected because ζ_c is a characteristic of the particle itself.

Table 3. Summary of Model Parameters for Invitrogen Ultra Pure Agarose Gels for 1× TAE (42 mM, top) and 0.25× TAE (10.5 mM, bottom) Experiments with Agarose Gel Segment MWs $n_g = 10^3$ and 10^4 kDa[a]

M_g (kDa)	u_f (μm s^{-1})	κ^{-1} (nm)	ζ_c (mV)
10^3	540	3.0	−64
10^4	68	2.8	−60
10^3	425	5.8	−64
10^4	50	5.1	−59

[a] M_g = Agarose gel segment MW. u_f = NP−hydrogel frictional coupling velocity parameter. κ^{-1} = Debye length. ζ_c = Au NP core ζ-potential (*bare* Au NP).

The differences between the measured and calculated (fitted) mobilities in Figure 3 may reflect experimental conditions that are unaccounted for in the theoretical model. However, it is clear that electroosmosis plays a fundamental role in NP migration. From this work, we draw several interesting conclusions. First, NP mobilities are strongly affected by the surface ligand. Our observations agree with Liu et al.,[31] Perrault and Chan,[32] and Hanauer et al.,[20] who identified a mobility reversal when increasing PEG ligand grafting density. Here we focused on how the PEG−ligand MW affects NP electromigration properties, demonstrating that ligand length can radically alter NP mobility. Note that uncharged polymer ligands with MW < 1 kDa yield functionalized Au NPs that migrate toward the positive electrode with highest electrophoretic mobility.

Second, we identify distinct MW regimes with vanishing electrophoretic mobility. Figure 3a shows distinct PEG MWs (∼2.0 kDa for 42 mM and ∼2.5 kDa for 10.5 mM ionic strength) where the NP mobility vanishes at any hydrogel concentration. This explains why 2 kDa PEGylated Au NPs are notoriously immobile: the electrophoretic and electro-osmotic

(54) Johnson, E. M.; Deen, W. M. *AIChE J.* **1996**, *42*, 5–1220.

forces balance to yield zero translation. Interestingly, the theory also identifies a PEG−ligand MW (∼2.3 and ∼3.9 kDa for 42 and 10.5 mM ionic strength, respectively) where the mobility is independent of the agarose concentration (dashed lines in Figure 3).

Third, fitting the model to experimental data shows that the Au NP core ζ-potential does not change appreciably with ionic strength. This is consistent with the expectation of the Au NP core being inert. The theory accounts for the hydrodynamic screening of the PEG ligand decreasing the apparent NP ζ-potential. It is important to note that DLS-microelectrophoresis experiments also reveal an apparent NP potential in free solution (Ohshima's formula eq 13). For NPs bearing long-grafted polymer chains, such as PEG, significant increases in hydrodynamic drag and frictional coupling with the gel are expected. These can be erroneously interpreted as a decrease in NP ζ-potential in all manner of soft NP electrophoresis experiments.

Conclusion

We presented experiments and an accompanying theoretical model to quantify the electrophoretic mobility of PEGylated Au NPs in agarose hydrogels, accounting for electrical, hydrodynamic, and frictional coupling forces. Adopting several reasonable simplifications, we derived a simple, closed-form solution of a more general electrokinetic model that captures several notable characteristics of the experimental data; in particular, the previously unexplained possibility of negatively charged Au NPs migrating as if they bear a positive charge. Increasing the PEG−ligand MW decreased the apparent Au NP core surface charge but increased the hydrodynamic drag and frictional coupling forces. The theory clearly identified PEG−ligand MWs where the NP mobility changes sign, even if the particle charge remains constant. Finally, the theoretical interpretation of experiments furnished previously unknown model parameters, including the Au NP core ζ-potential, PEG-layer hydrodynamic permeability, and frictional coupling coefficient. More generally, we hope that our research lends confidence to a robust and predictive model that might be adopted for a broader class of NP gel electrophoresis diagnostic technologies using tailored NPs.

Acknowledgment. R.J.H. gratefully acknowledges support from the Natural Sciences and Engineering Research Council of Canada and the Canada Research Chairs program. C.B. wishes to thank Dr. Daniel Scherson for insightful discussions of Au surfaces in electrolyte solutions.

Supporting Information Available: Further discussion of DLS, DLS-microelectrophoresis, and TGA is supplied in additional pages. This material is available free of charge via the Internet at http://pubs.acs.org.

JA1049093